J. Fluid Mech. (1981), *vol.* 109, *pp.* 45–61
Printed in Great Britain

Numerical simulation of relative dispersion in two-dimensional, homogeneous, decaying turbulence

By A. D. KOWALSKI AND R. L. PESKIN

Department of Mechanical, and Aerospace Engineering, Geophysical Fluid Dynamics Program, Rutgers University, New Brunswick, New Jersey, 08903

(Received 26 November 1979 and in revised form 31 March 1980)

Lagrangian statistical results are presented from numerical simulations of an ensemble of fluid particles which were generated from a two-dimensional pseudospectral code. The single-particle results are in qualitative agreement with previous simulations on a lower-resolution grid. The two-particle, relative velocity correlations were found to fall off more rapidly than the single-particle correlations for short to intermediate times due to large-scale eddy advection in the single-particle case. The temporal behaviour of the mean square relative separation, $\langle r_{\rm rel}^2 \rangle$, is analysed for short to intermediate times and is found to be consistent with scaling arguments based on Kraichnan's expression for the non-local strain acting in the high-wavenumber enstrophy cascade spectral range. For longer times, $\langle r_{\rm rel}^2 \rangle$ exhibits t^n behaviour. The power-law region is associated with the locally determined strain rates which characterize a backward energy-cascade spectrum.

1. Introduction

While the study of dispersion phenomena in two-dimensional turbulence is interesting as a check on concepts regarding dispersion in three-dimensional turbulence (e.g. scaling, localness of transfer processes), practical concern for the problem stems from the fact that, over a large range of length scales, motions in the atmosphere may be regarded as 'quasi'-two-dimensional (Charney 1971). Thus, studies of dispersion in a two-dimensional turbulence model should provide valuable information pertaining to atmospheric flows, and possibly oceanic flows.

Previous studies in dispersion phenomena have centred primarily on the single-particle problem in two and three dimensions and on the two-particle problem in three dimensions. Monin & Yaglom (1971) and Tennekes & Lumley (1972) review the basic principles of the subject. Numerical simulation studies of the process have been presented by Deardorff & Peskin (1970) and Peskin (1974), while theoretical models have been developed by Pismen & Nir (1978) and Kraichman (1974) among others. Although it is well known that Richardson's t^3 law applies to the average squared relative separation in three dimensions, the situation in two dimensions has been less clear. In the inertial sub-range in three dimensions, the straining of eddies (a source of relative motion) is primarily a local interaction in that eddies of a given size are being strained, for the most part, by only slightly larger eddies (Tennekes & Lumley 1972). In two dimensions, however, the strain rate interactions appear to be partially non-locally determined for the smaller scales in the field and more locally determined for

larger scales (Kraichnan 1971). Thus one would expect a difference in behaviour for the mean square relative separation between the range of scales over which the strain rate appears nearly constant with respect to relative distance (or wavenumber) and those larger scales where the strain rate becomes dependent on the relative distance over which it acts. The present study is an attempt to clarify the relative dispersion problem for two-dimensional turbulence by obtaining Lagrangian fluid particle trajectory statistics from a numerically integrated turbulent flow field. Lagrangian relative velocity correlations and dispersion rates are obtained by averaging over an ensemble of fluid particles. The results are then analysed with some simple scaling arguments.

2. Description of the Eulerian field simulation

The technique for the simulation of the two-dimensional flow field is due to Orszag (1976). The system of equations employed is the familiar stream function–vorticity formulation of the Navier–Stokes equations for two-dimensional incompressible flows. I.e.

$$\left.\begin{aligned}\frac{\partial \zeta}{\partial t} &= \frac{\partial(\zeta,\psi)}{\partial(x,y)} + \nu\nabla^2\zeta \\ &= \frac{\partial\psi}{\partial y}\frac{\partial\zeta}{\partial x} - \frac{\partial\psi}{\partial x}\frac{\partial\zeta}{\partial y} + \nu\nabla^2\zeta,\end{aligned}\right\} \tag{2.1}$$

where $\zeta(x,y,t)$ is the vorticity, $\psi(x,y,t)$ is the stream function and the two are related by

$$\zeta = -\nabla^2\psi. \tag{2.2}$$

For a homogeneous flow, the appropriate boundary conditions are periodic, i.e.

$$\begin{aligned}&\zeta(x+2\pi n, y+2\pi m, t) = \zeta(x,y,t),\\ &\psi(x+2\pi n, y+2\pi m, t) = \psi(x,y,t) \quad (n,m = 0, \pm 1, \ldots)\end{aligned} \tag{2.3}$$

and ζ and ψ may be expanded in Fourier series to yield the spectral forms of (2.1) and (2.2):

$$\left.\begin{aligned}\frac{\partial\hat{\zeta}(p,q,t)}{\partial t} &= N(p,q,t) - \nu(p^2+q^2)\,\hat{\zeta}(p,q,t),\\ \hat{\zeta}(p,q,t) &= (p^2+q^2)\,\hat{\psi}(p,q,t).\end{aligned}\right\} \tag{2.4}$$

$N(p,q,t)$ is the Fourier transform of the nonlinear term in (2.1) and it is given by

$$N(p,q,t) = \sum_{p',q'} (p'q - pq')\,\hat{\zeta}(p',q',t)\,\hat{\psi}(p-p',q-q',t), \tag{2.5}$$

with $\qquad |p'| < P, \quad |q'| < Q, \quad |p-p'| < P \quad \text{and} \quad |q-q'| < Q.$

P and Q are the maximum wavenumbers used in the simulations. In our computer runs these were taken to be $P = Q = 64$ for the preliminary runs and $P = Q = 256$ for the final run, corresponding to 128×128 and 512×512 physical space grids respectively.

The scheme represented by (2.4) with boundary conditions (2.3) is solved by an efficient pseudospectral method which fast Fourier transforms the factors in the nonlinear terms into real space, multiplies them, and transforms the result back into Fourier space without having to evaluate (2.5) directly. Aliasing errors are eliminated

	128×128		512×512	
	$t = 0$	$t = 2{\cdot}0$	$t = 0$	$t = 2{\cdot}0$
Large-scale Reynolds number, R	800	600	21 000	8500
Total enstrophy, Ω	19·8	12·5	20·9	18·3
Total energy, E_{TOT}	0·97	0·93	1·22	1·23
Dissipation wavenumber, k_d	34·9	38·9	75·6	119
Viscosity, ν	0·001		0·0001	
Time step, Δt	0·004		0·001	
Initial injection wavenumber, k_0	$\frac{3}{2}$		$\frac{3}{2}$	

TABLE 1. Eulerian field parameters.

with an efficient truncation scheme (Patterson & Orszag 1971). The time marching of (2.4) is accomplished by using a leap-frog scheme for the nonlinear term and a Crank–Nicholson scheme for the diffusive term.

The initial values of the Fourier components of the stream function field were chosen to be Gaussian distributed with an initial energy spectrum given by

$$E(k) = v_0^2(k/k_0)\exp(-k/k_0), \tag{2.6}$$

with $v_0 = 1$ and $k_0 = \frac{3}{2}$. The scales of v_0 and the box length $d = 2\pi$ determine the basic units of length and time for the measurements reported here. This initialization procedure does not guarantee isotropy in the larger scales of the field so that the simulation should be considered to be one realization of an isotropic ensemble.

The band-averaged modal energy-spectrum coefficient is measured as

$$E(k) = \sum_{|\mathbf{k}|} |\mathbf{k}|^2 \hat{\psi}(\mathbf{k})\,\hat{\psi}(\mathbf{k})^*, \quad k - \tfrac{1}{2}\Delta k \leqslant |\mathbf{k}| < k + \tfrac{1}{2}\Delta k \tag{2.7}$$

and the enstrophy spectrum as

$$\Omega(k) = \sum_{|\mathbf{k}|} |\mathbf{k}|^4 \hat{\psi}(\mathbf{k})\,\hat{\psi}(\mathbf{k})^*, \quad k - \tfrac{1}{2}\Delta k \leqslant |\mathbf{k}| < k + \tfrac{1}{2}\Delta k, \tag{2.8}$$

with $\mathbf{k} = (p, q)$ and Δk equal to the bandwidth. The total energy is then

$$E_{\mathrm{TOT}} = \sum_k E(k)\,\Delta k, \tag{2.9}$$

and the Reynolds number may be defined as

$$R = E_{\mathrm{TOT}}/(\nu\eta^{\frac{1}{3}}) \tag{2.10}$$

with η equal to the enstrophy dissipation rate. The relevant parameters for both the preliminary 128×128 and final 512×512 simulations are given in table 1. For simplicity, the 128×128 run will be labelled as $R128$ and the 512×512 run will be labelled $R512$ in most of what follows.

3. Eulerian field results

Batchelor (1969) and Kraichnan (1967) have postulated that two-dimensional turbulence should display two distinct asymptotic spectral regions for large Reynolds numbers. If energy and enstrophy are injected into the flow around a given wavenumber, k_0 say, then the net transport of energy is towards wavenumbers less than k_0

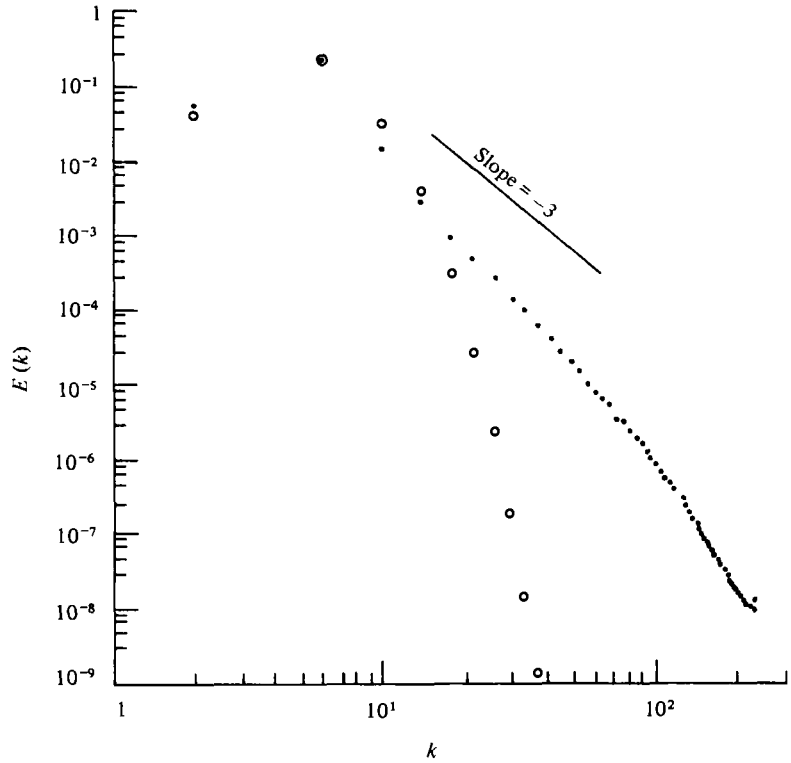

FIGURE 1. Energy spectra for $R512$. Circles are the initial spectrum. Points are the spectrum at $t = 2{\cdot}08$.

and the net transport of enstrophy is towards wavenumbers greater than k_0 up to $k_d = (\eta/\nu^3)^{\frac{1}{6}}$, beyond which enstrophy is dissipated at rate η.

The proposed asymptotic forms for these two spectral regions are

$$E(k) = c\epsilon^{\frac{2}{3}}k^{-\frac{5}{3}} \quad (k < k_0) \tag{3.1}$$

for the backward energy-cascade region of the spectrum and

$$E(k) = c'\eta^{\frac{2}{3}}k^{-3} \quad (k > k_0) \tag{3.2}$$

for the enstrophy cascade region; ϵ is the rate at which energy is transferred through the $k^{-\frac{5}{3}}$ region of the spectrum.

Other proposed forms for the enstrophy cascade spectrum include a k^{-4} spectrum (Saffman 1971) and a logarithmically corrected k^{-3} spectrum (Kraichnan 1971). Figure 1 shows the energy spectrum that evolved for $R512$ at $t = 2{\cdot}08$ along with the initial energy spectrum. The results, averaged over wavenumber bands of width $\Delta k = 4$, indicate a build-up of energy in the low-wavenumber region with sufficient transport of energy to the right to allow enstrophy to be transferred to high wavenumbers (the net transport of energy being to the left). This was expected since there is no mechanism in the model for the removal of energy at low wavenumbers nor for the injection of energy and enstrophy at intermediate wavenumbers. The empirical result shown in figure 1 does not indicate a clear choice between a logarithmically corrected k^{-3} spectrum and a k^{-4} spectrum and, considering the difficulties in achieving

asymptotic spectral levels even in high-resolution experiments, the results cannot be considered to be a confirmation of any particular proposed asymptotic spectrum. In spite of this restriction, however, $R512$ does yield a self-similar enstrophy cascade spectral region of approximately asymptotic form and much can be said about the relative separation process over distances corresponding to that region. Moreover, because of the energy and enstrophy conservation constraints which apply to two-dimensional turbulence (Batchelor 1953), there is a local interaction reverse energy-cascade spectral region, although it is neither asymptotic nor self-similar in this simulation.

Vorticity maps for $R512$ are shown in figure 2(a, b) at times $t = 0{\cdot}04$ and $t = 1{\cdot}24$ respectively. The contour intervals at both times were the same and the results were reduced to 128×128 grid points by taking every fourth point in x and y. The vorticity contours qualitatively illustrate the amplification of vorticity gradients which occurs in two-dimensional turbulence; i.e. the transfer of vorticity to smaller scales (Batchelor 1969).

The results for the enstrophy dissipation rate η and total enstrophy Ω as a function of time are shown in figures 3(a) and (c) respectively: η is generally larger for $R128$ than for $R512$ since the viscosity is ten times larger for the lower-resolution run. The total enstrophy for $R512$ decayed by about 14 % of its initial value over the time of the simulation compared with 36 % for $R128$ for the same period.

A two-dimensional skewness may be defined by

$$S = -2\left\langle \frac{\partial v_1}{\partial x}\left(\frac{\partial \zeta}{\partial x}\right)^2\right\rangle \Big/ \left(\left\langle \left(\frac{\partial v_1}{\partial x}\right)^2\right\rangle^{\frac{1}{2}} \left\langle \left(\frac{\partial \zeta}{\partial x}\right)^2\right\rangle\right), \tag{3.3}$$

where ζ is the vorticity (Herring *et al.* 1974). S is a measure of the rate of production of mean square vorticity gradients by nonlinearity and its levelling off in time indicates that the decay at large wavenumbers has become self-similar. Figure 3(b) shows the variation of S with time for $R512$ and it indicates that large-wavenumber self-similarity occurred at about $t = 0{\cdot}6$.

4. Simulation of the Lagrangian field

Lagrangian fluid-particle statistical information for the flow field was obtained by numerically integrating the equation for the fluid-particle trajectories

$$\mathbf{v}(\mathbf{a}, t) = \frac{\partial}{\partial t}\mathbf{X}(\mathbf{a}, t) = \mathbf{U}(\mathbf{X}(\mathbf{a}, t), t), \tag{4.1}$$

where $\mathbf{v}(\mathbf{a}, t)$ is the Lagrangian velocity of a fluid particle at time t which was at position $\mathbf{a}$ at time $t = 0{\cdot}0$. $\mathbf{X}(\mathbf{a}, t)$ is the particle's position at time t and $\mathbf{U}$ is the Eulerian field velocity at the particle's current position in the field at a given time. The velocity of a particle is then updated at the next time step using its new position and the time-stepped Eulerian velocity at that position. Velocities between grid points in the Eulerian field are retrieved by using a bivariate, four-point, linear interpolation scheme which collocates with the four surrounding grid points, i.e.

$$\begin{aligned}\mathbf{U}(x_i + \alpha h, y_j + \beta h, t) = (1-\alpha)(1-\beta)\,\mathbf{U}_{i,j} + \alpha(1-\beta)\,\mathbf{U}_{i+1,j} + \beta(1-\alpha)\,\mathbf{U}_{i,j+1} \\ + \alpha\beta\,\mathbf{U}_{i+1,j+1} + O(h^2),\end{aligned} \tag{4.2}$$

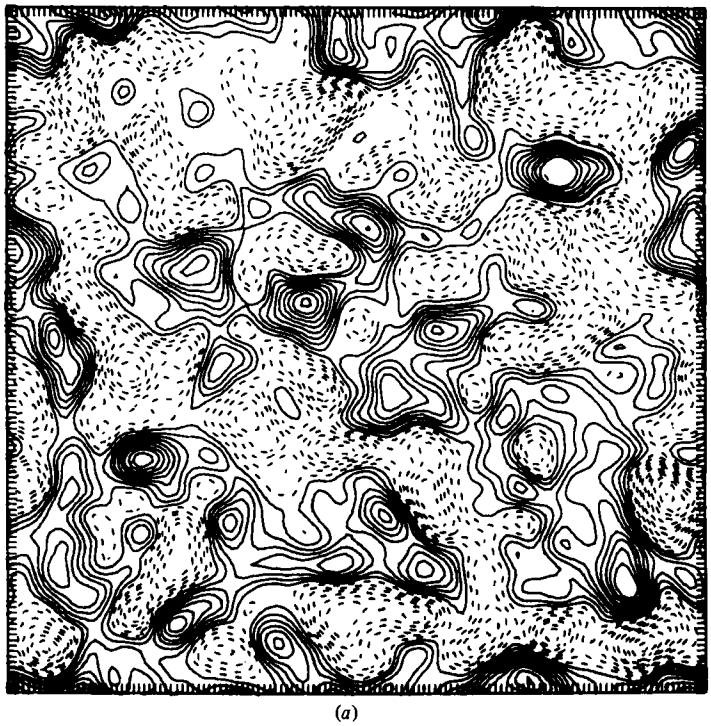

(*a*)

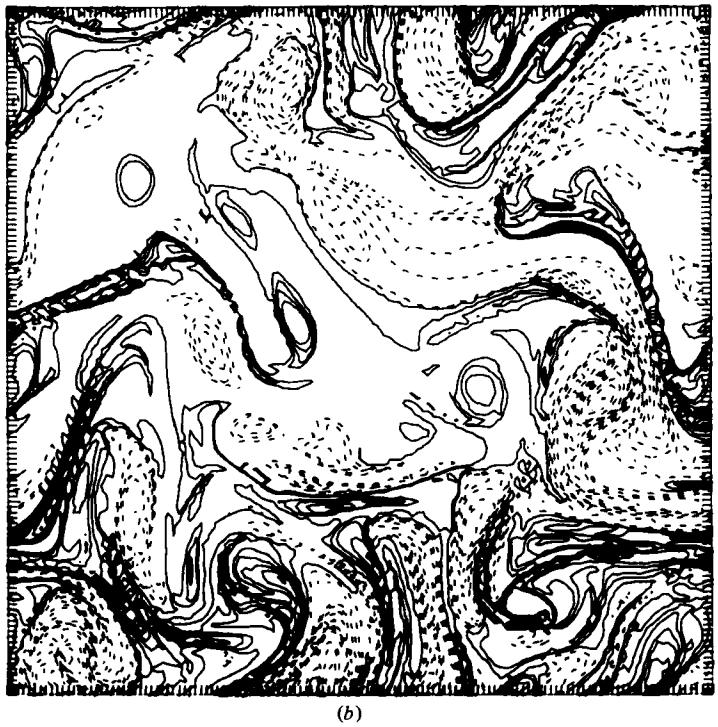

(*b*)

FIGURE 2. Vorticity contours for $R512$ at (*a*) $t = 0{\cdot}04$ and (*b*) $t = 1{\cdot}24$.

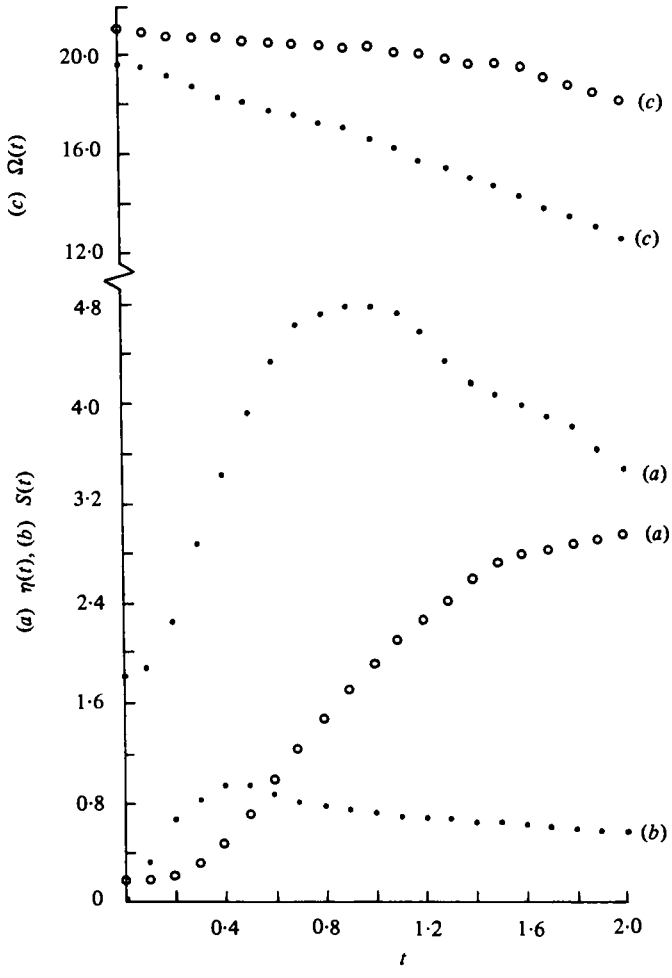

FIGURE 3. Eulerian field variables: (*a*) enstrophy dissipation rate for $R512$ (circles) and $R128$ (points), (*b*) skewness, (*c*) enstrophy for $R512$ (circles) and $R128$ (points).

where $\mathbf{U}_{i,j} \equiv \mathbf{U}(x_i, y_j, t)$ is an Eulerian velocity component at (x_i, y_j),

$$h = |x_{i+1} - x_i| = |y_{i+1} - y_i|$$

is the grid interval and α and β are the fractional grid displacements in the x and y directions respectively.

Statistical information regarding the Lagrangian field was obtained by averaging over an ensemble of 1024 fluid elements which were initially placed in a 32×32 rectangular array on the computational grid. The initial spacing between adjacent pairs of elements was 12 grid intervals for $R512$ and 3 grid intervals for $R128$, corresponding to an initial separation distance of $|\mathbf{A}| = 0{\cdot}147$ for each of the 1984 possible adjacent particle pairs in the simulation. This distance matches a wavenumber of about $k \simeq 2\pi/|\mathbf{A}| \simeq 43$, which is considered to be at the high-wavenumber end of the enstrophy cascade region of the energy spectrum for the larger simulation. Because of the cyclic nature of the boundary conditions, particles which wandered outside the

box $0 \leqslant x < 2\pi$, $0 \leqslant y < 2\pi$ were assigned Eulerian velocities corresponding to their positions modulo the box size. For example,

$$\left.\begin{aligned} U(x,y,t) &= U(x \bmod (2\pi), y \bmod (2\pi), t), \quad (x \geqslant 0,\ y \geqslant 0), \\ U(x,y,t) &= U(x \bmod (2\pi) + 2\pi, y \bmod (2\pi) + 2\pi, t), \quad (x < 0,\ y < 0). \end{aligned}\right\} \tag{4.3}$$

The particle tracking was begun at $t = 0{\cdot}6$, the time at which the two-dimensional skewness factor defined in § 3 began to level off. The initial velocity of each particle was that of the Eulerian field at its initial position.

5. Lagrangian results

(*a*) *Single-particle statistics*

The Lagrangian single-particle statistics for two-dimensional turbulent flows were analysed previously by Peskin (1974) using a $(64)^2$ grid size Eulerian field simulation developed by Lilly (1969, 1972). The measured single-particle results from the present simulation are comparable and are presented for qualitative contrast to the two-particle results presented below.

The Lagrangian single-particle velocity auto-correlation, a measure of the degree of correlation of a fluid particle's velocity at time t with its velocity at a later time $t+\tau$, is defined as

$$\rho_i^{\mathrm{sgl}} = \frac{\langle v_i(\mathbf{a},t)\, v_i(\mathbf{a},t+\tau)\rangle}{\langle v_i^2(\mathbf{a},t)\rangle^{\frac{1}{2}}\, \langle v_i^2(\mathbf{a},t+\tau)\rangle^{\frac{1}{2}}}, \tag{5.1}$$

where the brackets denote ensemble averages over the set of 1024 fluid particles. Figure 4(*b*) is a plot of ρ_1^{sgl} *vs.* τ for the $(512)^2$ run up to the final tracking time of $\tau = 1{\cdot}48$ and figure 5(*b*) shows ρ_1^{sgl} for the $(128)^2$ run up to $\tau = 6{\cdot}0$ (the maximum lag time for $R128$ was $\tau = 8{\cdot}0$).

The correlations exhibit the characteristic parabolic shape at the origin but more important, although the correlations show a continuously decreasing average value with superimposed fluctuations, the curves retain mean positive behaviour for a rather prolonged period. This indicates that the single-particle statistics are strongly characterized by the mean advective effects of the largest eddies in the flow. That is, the particles are being swept along by the mean, unidirectional velocities characteristic of the large eddies until sufficient time has elapsed to allow the large-scale features of the flow to change. This is further corroborated by a measurement of the mean square single-particle displacement *vs.* time, $\langle r_{\mathrm{sgl}}^2\rangle = \langle X_1^2\rangle + \langle X_2^2\rangle$, depicted in figure 6(*b*) on a log–log scale. The initial t^2 dependence indicates that the particles are being carried along at a relatively constant velocity for short times after release. For very large times the curve approaches a linear dependence on $\hat{t} = t - 0{\cdot}6$, indicating statistical independence and lack of correlation in the particle velocities. The results are consistent with Taylor's (1921) ideas of single-particle dispersion and a spectral formulation of the problem (Batchelor 1950) which clarifies the importance of the low-wavenumber eddies in single-particle dispersion.

The correlation fluctuations observed in figure 5 at $\tau = 1{\cdot}8$ might possibly be due to the large-scale anisotropy in the field. We have not identified any specific physical basis for these fluctuations.

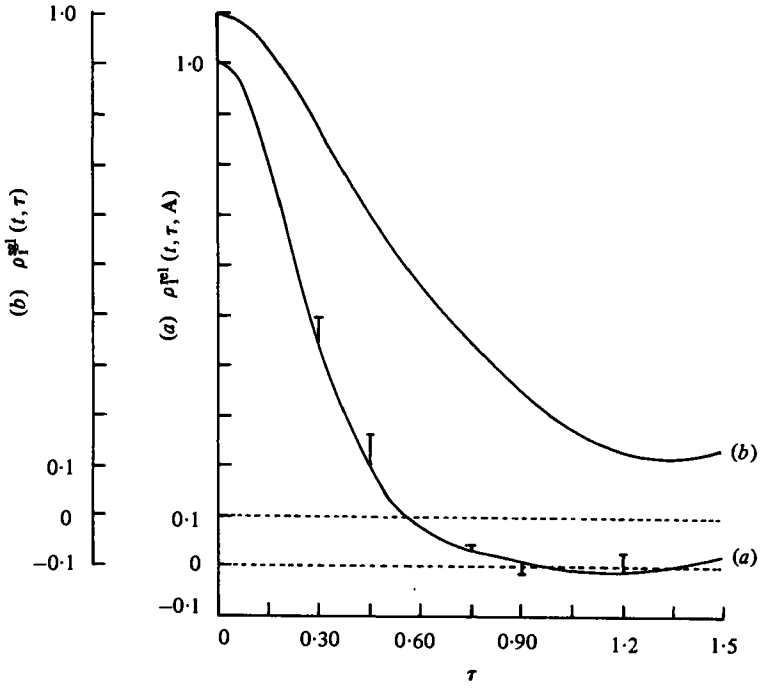

FIGURE 4. Lagrangian velocity auto-correlation for $R512$ for (*a*) relative dispersion and (*b*) single-particle dispersion.

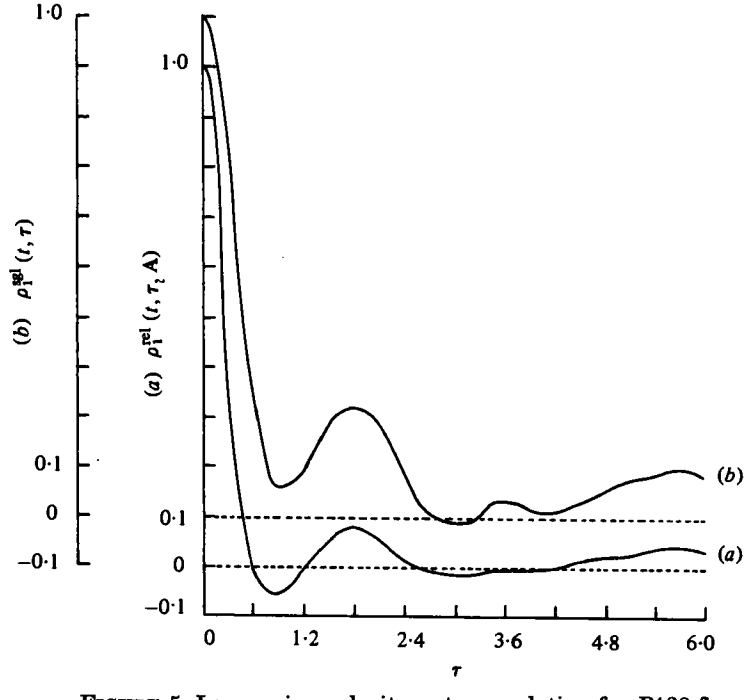

FIGURE 5. Lagrangian velocity auto-correlation for $R128$ for (*a*) relative dispersion and (*b*) single-particle dispersion.

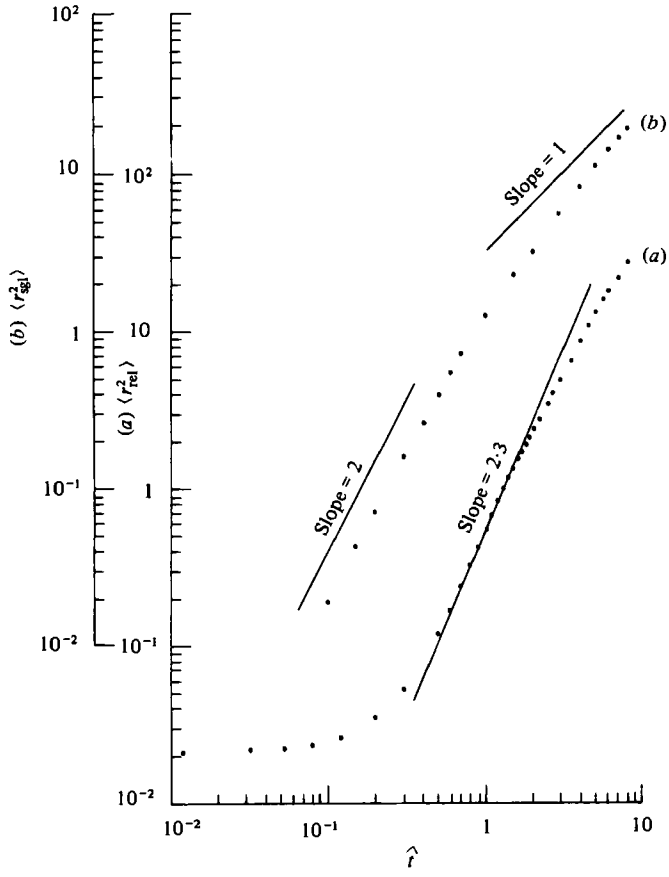

FIGURE 6. (*a*) Mean square relative displacement for $R128$ and (*b*) mean square single-particle displacement for $R128$.

(*b*) *Two-particle results*

The difference between the statistics of single-particle and two-particle systems is similar to the situation in the classical treatment of systems of particles in which the motions of pairs of particles are resolved into a centre-of-mass motion and a relative motion. Taking the difference in the trajectories or velocities of pairs of particles effectively eliminates the common motion between them, revealing the more physically significant internal interactions between fluid parcels. Figures 4(*a*) and 5(*a*) show plots of the relative velocity auto-correlation coefficient *vs.* time defined by

$$\rho_i^{\mathrm{rel}} = \frac{\langle w_i(\mathbf{A},t)\, w_i(\mathbf{A},t+\tau)\rangle}{\langle w_i^2(\mathbf{A},t)\rangle^{\frac{1}{2}} \langle w_i^2(\mathbf{A},t+\tau)\rangle^{\frac{1}{2}}}, \tag{5.2}$$

where $w_i = v_{ai} - v_{bi}$ is the ith component of the difference velocity between particles a and b in a pair. The brackets denote an ensemble average over the 1984 initially adjacent particle pairs of initial separation $\mathbf{A}$. Comparison with figures 4(*b*) and 5(*b*) shows a much more rapid fall-off in the dual particle correlations reflecting the absence of enhancement due to mean advection by large-scale eddies which characterized the single-particle problem for small to intermediate times.

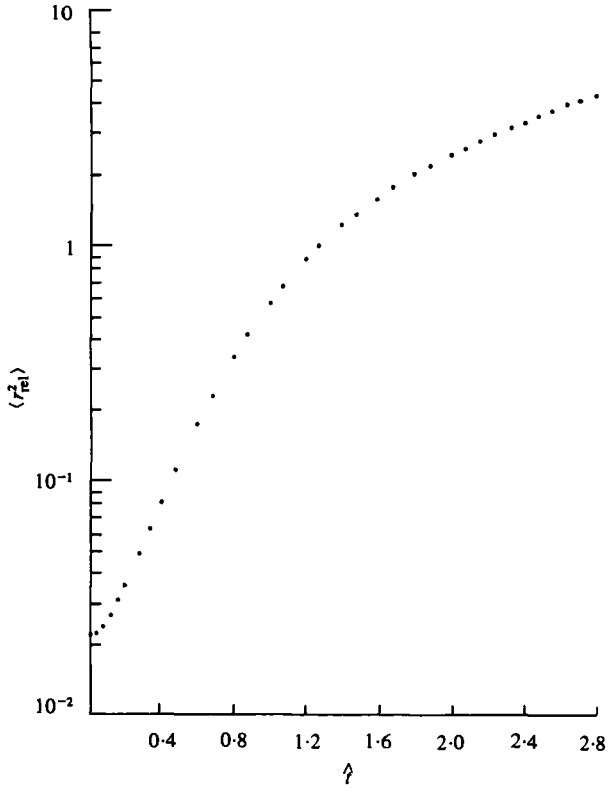

FIGURE 7. Mean square relative displacement for $R128$.

The mean square relative separation is $\langle r_{\rm rel}^2 \rangle = \langle Y_1^2 \rangle + \langle Y_2^2 \rangle$ with $Y_i = Y_{ai} - Y_{bi}$ and $\langle Y_i^2 \rangle$ is related to $\rho_i^{\rm rel}$ by

$$\frac{1}{2}\frac{d\langle Y_i^2 \rangle}{dt} = \int_0^t \langle w_i^2(\mathbf{A}, t)\rangle^{\frac{1}{2}} \langle w_i^2(\mathbf{A}, t+\tau)\rangle^{\frac{1}{2}} \rho_i^{\rm rel}(t, \tau, \mathbf{A})\, d\tau. \tag{5.3}$$

The variation of $\langle r_{\rm rel}^2 \rangle$ in time for the $(128)^2$ run is plotted in figures 6(a) and 7. Figure 7 shows a short exponential region from $\langle r_{\rm rel}^2 \rangle = 0{\cdot}03$ to $0{\cdot}17$ corresponding to wavenumbers $k = 36$ to 15 and times $\hat{t} = 0{\cdot}16$ to $\hat{t} = 0{\cdot}6$ respectively. For larger times, figure 6(a) indicates that the average squared relative separation changes over to t^n behaviour, where n reached a maximum of approximately 2·3 between $\langle r_{\rm rel}^2 \rangle = 0{\cdot}28$ and 1·4 corresponding to wavenumbers 12 to 5 and times 0·7 to 2·0 respectively. For very large times, and separation distances slightly less than the box size, $\langle r_{\rm rel}^2 \rangle$ appears to be approaching a linear dependence on $\hat{t}$, indicating that, on the average, the two material points in each pair are wandering independently. The behaviour of $\langle r_{\rm rel}^2 \rangle$ for short to intermediate times may be analysed in terms of the effective strain rate acting on an eddy of size $\delta r \sim \langle r_{\rm rel}^2 \rangle^{\frac{1}{2}}$ insofar as the turbulence may be regarded as isotropic. A quantitative analysis is taken up below.

The probability distributions of relative displacements in the x direction, $p_1^{\rm rel}(t, \hat{t}, s)$ of the pair ensemble at trajectory times $\hat{t} = 0{\cdot}25$ and $\hat{t} = 1{\cdot}37$ are depicted in figures 8(a) and (b) as a function of the standard deviations s at those times. Compared to Gaussian distributions of the same standard deviation, the curves indicate that the particle pairs

spend relatively little time (low probability) in portions of the distributions corresponding to rapid separation rates. The Gaussian distribution represents a linear dependence of $\langle r_{\rm rel}^2 \rangle$ on time corresponding to statistically independent random motion for each particle in a pair.

Figure 9 shows $\langle w_{\rm rel}^2 \rangle$, the total relative mean square velocity, as a function of time. In particular, if we assume that $\langle w_{\rm rel}^2 \rangle \sim (d(\delta r)/dt)^2$ (which implies weak correlation between relative displacement and relative acceleration) then the results show that $\langle w_{\rm rel}^2 \rangle$ develops exponential and power-law regions at times corresponding to similar regions for $\langle r_{\rm rel}^2 \rangle$. In the power-law region of figure 9 (from about $\hat{t} = 0{\cdot}7$ to $2{\cdot}0$), $\langle w_{\rm rel}^2 \rangle \sim t^{0{\cdot}6}$, whereas one would expect an exponent of about $\frac{1}{3}$ from the scaling estimate.

6. Analysis of the relative separation

Kraichnan (1971) has given a simple dynamical argument which leads to a logarithmically corrected k^{-3} energy spectrum for the enstrophy cascade range in two-dimensional isotropic turbulence. The correction preserves a constant, k-independent enstrophy transfer rate and compensates for the effect of the non-local nature of the enstrophy transfer process on the form of the energy spectrum. Kraichnan assumes that the effective strain rate $\omega(k)$ acting to distort eddies of scale $1/k$ is given by

$$\omega^2(k) \sim \int_{k_0}^{k} p^2 E(p)\, dp, \tag{6.1}$$

since effects of wavenumbers $\gg k$ should average out over scales $1/k$ and times $\omega^{-1}(k)$. In fact, the validity of this argument depends strongly on the form of $E(k)$. For a k^{-3} spectral range, however, ω^2 diverges logarithmically for small k_0, which suggests that the major contribution to the integral in (6.1) comes from wavenumbers $< k$ and that the straining process is strongly non-local for eddies at large wavenumbers.

It is useful to employ Kraichnan's expression for the energy spectrum

$$E(k) = D\eta^{\frac{2}{3}} k^{-3} \left[\ln\left(\frac{k}{k_0}\right)\right]^{-\frac{1}{3}} \quad (k \gg k_0)$$

in (6.1) in order to illustrate analytically the overall dependence of ω^2 on k and its effect on the behaviour of the mean square relative separation in time. This yields

$$\omega^2 = \tfrac{3}{2} D' \eta^{\frac{2}{3}} \left[\ln \frac{k}{k_0}\right]^{\frac{2}{3}}, \tag{6.2}$$

where the proportionality constants have been absorbed into D'. A rough numerical calculation of ω^2 was also obtained from the band-averaged points of the spectrum in figure 2 in the region of interest ($k \sim 5$–36) and the behaviour is comparable to that of (6.2).

Given that the vorticity of each fluid element is an invariant of the motion in two-dimensional turbulence, it seems reasonable to associate the relative velocity of particle pairs with the transfer of enstrophy in the enstrophy cascade range, since it is a relative velocity which causes a change in scale from one wavenumber to another. This implies that the relative velocity in a similarity enstrophy cascade range should

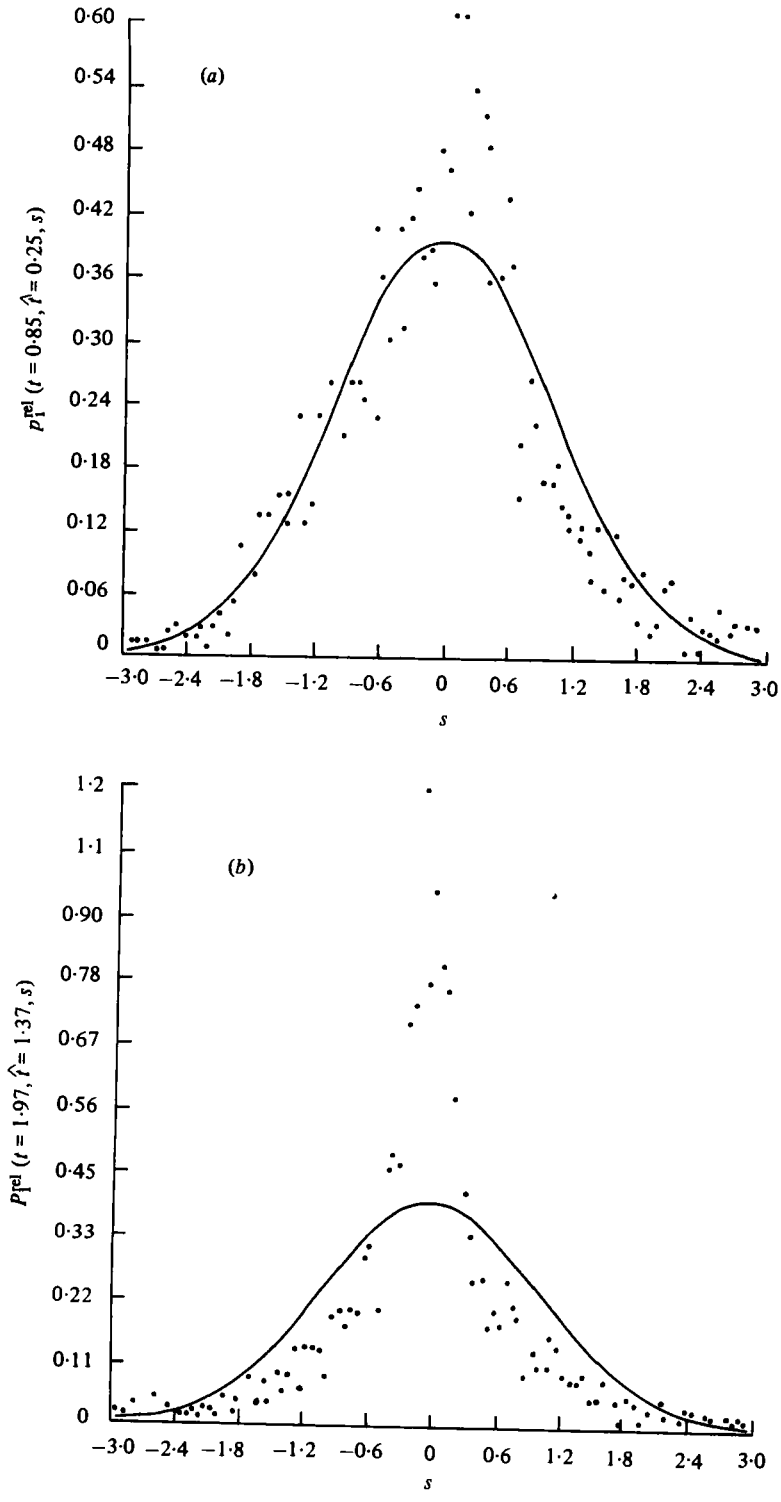

FIGURE 8. Probability density distribution of relative displacements for $R128$ at (*a*) $\hat{t} = 0{\cdot}25$ and (*b*) $\hat{t} = 1{\cdot}37$.

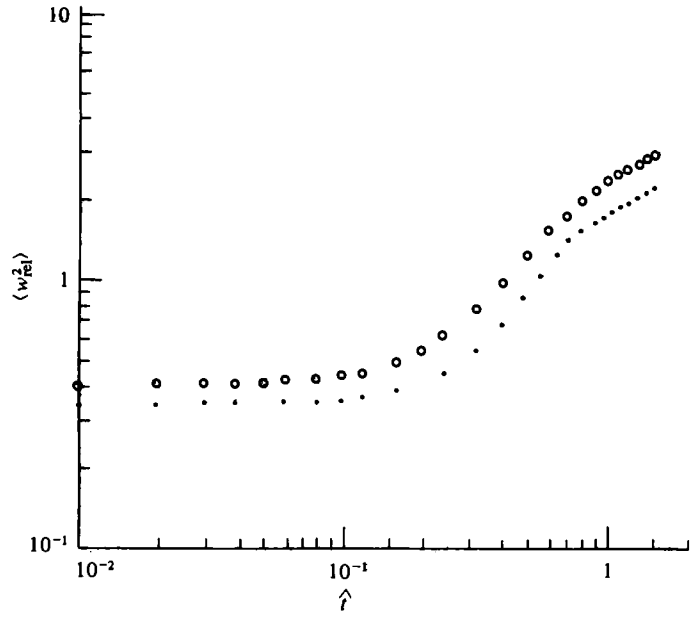

FIGURE 9. Mean square relative velocity for $R128$ (points) and $R512$ (circles).

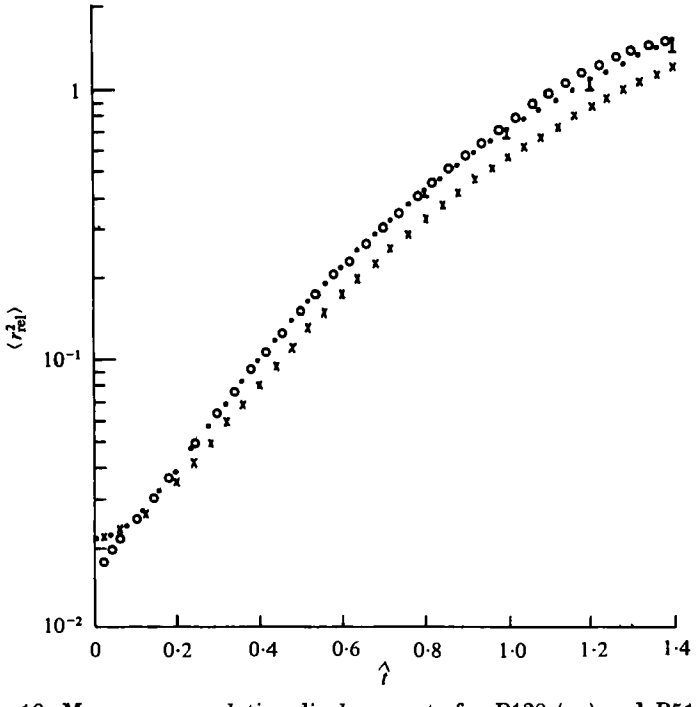

FIGURE 10. Mean square relative displacements for $R128$ (×) and $R512$ (points). The circles represent the approximation to the $R512$ data from (6.4).

depend only on the eddy size at a given wavenumber $\delta r \sim 1/k$ and the effective strain rate acting to distort eddies of that size, i.e.

$$w \propto \delta r\, \omega(\delta r). \tag{6.3}$$

Using (6.2) in (6.3) with $w \equiv d(\delta r)/dt$ yields an expression for the mean square relative separation

$$\langle r_{\rm rel}^2 \rangle \equiv (\delta r)^2 = (\delta r_0)^2 \exp\left(-2\{\tfrac{2}{3}(\tfrac{3}{2}D')^{\frac{1}{2}}\eta^{\frac{1}{3}}(\hat{t}_0 - \hat{t})\}^{\frac{3}{2}}\right) \quad (\delta r \ll \delta r_0) \tag{6.4}$$

Here $\hat{t}_0$ is the time required for an average pair to separate to the enstrophy injection size $\delta r_0 \sim 1/k_0$. The proportionality constant in (6.3) was absorbed into D'.

Given the asymptotic spectrum used, it is still instructive to compare (6.4) with the numerical results. Figure 10 shows (6.4) with the results from the $(512)^2$ simulation. $(\delta r_0)^2$ was chosen to be 1·52 at $\hat{t}_0 = 1{\cdot}4$ corresponding to $k \simeq 5$; near the lowest wavenumber for which a t^n region was observed. η was chosen to be 1·96 at the intermediate tracking time of $\hat{t} = 1{\cdot}0$ while D' was chosen to give a best fit for the smallest separation distances (high wavenumbers). Other choices for δr_0 and $\hat{t}_0$ give similar results with slightly varying values for D'. The value obtained for D' corresponding to the fit in figure 10 with $\eta = 1{\cdot}96$ was 1·46, which is somewhat lower than the energy spectrum coefficient, $D' = 2{\cdot}626$, computed by Kraichnan (1971) from an almost-Markovian Galilean-invariant turbulence model. If, on the other hand, η is chosen to be 1·0, its value at $\hat{t} = 0{\cdot}0$ (near the region where D' is chosen to give a best fit to the data) then we get the same theoretical curve in figure 10 but with $D' = 2{\cdot}28$.

The fit deviates from the experimental results near $\delta r_0 \sim 1/k_0$, where the strain rate $\omega(k)$, (6·1), is not expected to be accurate and near δr on the order of the initial separation distance. The latter deviation is due to the fact that the ensemble of pairs were released with identical separation distances and had not had sufficient time to develop a probability distribution that was not strongly dependent on the initial artificially spiked distribution. In general, however, (6.4) is a good overall fit to the data and it demonstrates explicitly through its dependence on δr_0 that the behaviour of the mean square particle separation for small to intermediate distances and times is not locally determined. It is also clear from (6.2) that, since $\omega(k)$ does not approach a constant value for $k \to \infty$, $\langle r_{\rm rel}^2 \rangle$ can never exhibit a pure $e^{\gamma t}$ (γ constant) behaviour corresponding to asympotically large k in an enstrophy cascade range.

For larger times and separations (6.4) indicates that $(\delta r)^2$ is influenced by locally controlled strain rates; i.e. $\omega^2(k)$ is a strong function of k. This leads to a t^n behaviour for $(\delta r)^2$. The possibility of the dependence of $\langle r_{\rm rel}^2 \rangle$ on local or non-local transfer mechanisms was pointed out by Peskin (1973). Specifically, it is conceivable that the strain present as a result of energy transfer in the smaller-wavenumber regions forms a large-scale strain field when observed from within the enstrophy transfer region. Thus, for smaller wavenumbers in the enstrophy transfer region, the relative separation process may be similar to the process in three dimensions with applied shear. In that case the mean square separation goes as t^3 (Corrsin 1959). For wavenumbers less than k_0, energy transfer is approximately local in two dimensions and one would also expect to observe t^3 behaviour for two-particle separations. In this context, it is interesting to note that the scheme represented by (6.1) and (6.3) with $k_0 = 0$ yields a t^3 dependency for $\langle r_{\rm rel}^2 \rangle$ for a $k^{-\frac{5}{3}}$ energy cascade spectrum. We emphasize, however, that only the tendency towards power-law behaviour was

observed experimentally and that the numerical results for the power-law region are not asymptotic. For long times and separations, this type of process would only hold until two points become statistically independent, at which time the mean square separation would be proportional to time.

The authors would like to thank Steven Orszag for his helpful discussions and the use of his KILOBOX code. Stimulating discussions with J. Herring are gratefully acknowledged. This research was supported by the Global Atmospheric Research Program, National Science Foundation (grants ATM76–18899 and ATM79–0164), and by the National Center for Atmospheric Research, which is sponsored by the National Science Foundation.

Appendix. Discussion of inaccuracies

Since it was not possible to obtain more than one realization of the Eulerian flow field due to the computational restriction imposed by the number of points to be processed in the $(512)^2$ run, the members of the ensemble of points (or pairs) are not necessarily statistically independent except over distances comparable to an integral length scale of the turbulent field. This type of error probably affects the large separation results more severely since there are fewer large-scale eddies on the field than small-scale ones. An experimental estimate of this type of error was obtained by repeating the statistical calculations using one quarter of the original number of particle pairs. The deviations in the statistics are shown as error bars in figures 4(*a*) and 10. First-order Taylor-series analysis indicates that errors due to interpolating the particle trajectories and velocities between grid points and time steps are no greater than the inaccuracies accumulated in the representation of the Eulerian field on the $(512)^2$ grid.

Technically, of course, (6.4) is applicable only to statistically steady (η constant) turbulence. Although a time-dependent η could have been included in the analysis in a continuous sense, it was felt that this would have unnecessarily masked the more important features of the analysis.

REFERENCES

BATCHELOR, G. K. 1950 The application of the similarity theory of turbulence to atmospheric diffusion. *Quart. J. Roy. Met. Soc.* **76**, 133.

BATCHELOR, G. K. 1953 *The Theory of Homogeneous Turbulence*. Cambridge University Press.

BATCHELOR, G. K. 1969 Computation of the energy spectrum in homogeneous two-dimensional turbulence. *Phys. Fluids Suppl.* **12**, II 233.

CHARNEY, J. C. 1971 Geostrophic turbulence. *J. Atmos. Sci.* **8**, 1087.

CORRSIN, S. 1959 Progress report on some turbulent diffusion research. *Advances in Geophysics*, vol. 6. Academic.

DEARDORFF, J. W. & PESKIN, R. L. 1970 Lagrangian statistics from numerically integrated shear flow. *Phys. Fluids* **13**, 584.

HERRING, J. R., ORSZAG, S. A., KRAICHNAN, R. H. & FOX, D. G. 1974 Decay of two-dimensional homogeneous turbulence. *J. Fluid Mech.* **66**, 417.

KRAICHNAN, R. H. 1967 Inertial ranges in two-dimensional turbulence. *Phys. Fluids* **10**, 1417.

KRAICHNAN, R. H. 1971 Inertial range transfer in two- and three-dimensional turbulence. *J. Fluid Mech.* **47**, 525.

KRAICHNAN, R. H. 1974 Convection of a passive scalar by a quasi-uniform random straining field. *J. Fluid Mech.* **64**, 737.

LILLY, D. K. 1969 Numerical simulation of two-dimensional turbulence. *Phys. Fluids Suppl.* **12**, II 240.

LILLY, D. K. 1972 Numerical simulation studies of two-dimensional turbulence. *Geophys. Fluid Dyn.* **3**, 289.

MONIN, A. A. & YAGLOM, A. M. 1971 *Statistical Fluid Mechanics.* Massachusetts Institute of Technology Press.

ORSZAG, S. A. 1976 Design of large hydrodynamic codes. *Proc. 3rd ICASE Conf. on Scientific Computing.* Academic.

PATTERSON, G. S. & ORSZAG, S. A. 1971 Spectral calculations of isotropic turbulence: efficient removal of aliasing interactions. *Phys. Fluids* **14**, 2538.

PESKIN, R. L. 1973 Comments on 'Relative dispersion in the enstrophy cascading inertial range of homogeneous two-dimensional turbulence'. *J. Atmos. Sci.* **30**, 733.

PESKIN, R. L. 1974 Numerical simulation of Lagrangian turbulent quantities in two and three dimensions. *Advances in Geophysics* A **18**. Academic.

PISMEN, L. M. & NIR, A. 1978 On the motion of suspended particles in stationary homogeneous turbulence. *J. Fluid Mech.* **84**, 193.

SAFFMAN, P. G. 1971 A note on the spectrum and decay of random two-dimensional vorticity distribution at large Reynolds number. *Studies Appl. Math.* **50**, 377.

TAYLOR, G. I. 1921 Diffusion by continuous movements. *Proc. Lond. Math. Soc.* A **20**, 196.

TENNEKES, H. & LUMLEY, J. L. 1972 *A First Course in Turbulence.* Massachusetts Institute of Technology Press.